ENVIRONMENTAL RESEARCH
LETTERS

LETTER

An analysis of roadside particulate matter pollution and population exposure over the Pearl River Delta region of China under clear-sky condition using new ultra-high-resolution $PM_{2.5}$ satellite-retrieval algorithms

Y Wu[1,2], H F Lee[1], R R Deng[3] and S H L Yim[4,5,6,*]

[1] Department of Geography and Resource Management, The Chinese University of Hong Kong, Sha Tin, Hong Kong Special Administrative Region of China, People's Republic of China
[2] Stanley Ho Big Data Decision Analytics Research Centre, The Chinese University of Hong Kong, Sha Tin, Hong Kong Special Administrative Region of China, People's Republic of China
[3] School of Geography and Planning, Sun Yat-sen University, Guangzhou, People's Republic of China
[4] Asian School of the Environment, Nanyang Technological University, Singapore, Singapore
[5] Lee Kong Chian School of Medicine, Nanyang Technological University, Singapore, Singapore
[6] Earth Observatory of Singapore, Nanyang Technological University, Singapore, Singapore
[*] Author to whom any correspondence should be addressed.

E-mail: yimsteve@gmail.com

Keywords: $PM_{2.5}$, AOD, ultra-high spatial resolution, Landsat-8, Pearl River Delta, roadside air quality

Supplementary material for this article is available online

OPEN ACCESS

RECEIVED
2 October 2023

REVISED
14 December 2023

ACCEPTED FOR PUBLICATION
13 February 2024

PUBLISHED
5 March 2024

Abstract

Roadside air pollution is one of the serious air pollution problems in urban areas. Even though roadside air pollution has been reported to cause adverse human health impacts, the spatial distribution of roadside air pollution in a large urban agglomeration has yet to be fully assessed. This study aimed to analyse roadside fine particulate matter ($PM_{2.5}$) pollution and the population exposure in 11 cities in the Pearl River Delta (PRD) region of China. We developed satellite-retrieval algorithms with dark target method, vector support machine model and random forest model to retrieve the spatial distribution of $PM_{2.5}$ at an ultra-high-spatial-resolution (30 m) based on 30 m Landsat-8 L1 data. Our results show that the retrieved $PM_{2.5}$ had a promising consistency with $PM_{2.5}$ measurements at general and roadside stations ($R^2 = 0.86$; RMSE $= 7.72\ \mu g\ m^{-3}$). Moreover, on average, the roadside $PM_{2.5}$ in Dongguan, Foshan, and Guangzhou was relatively higher (up to 107.60 $\mu g\ m^{-3}$) whereas that in Hong Kong was relatively lower (up to 30.40 $\mu g\ m^{-3}$). The roadside $PM_{2.5}$ pollution typically occurred in roads for motorized vehicles i.e. motorway, trunk, primary and secondary road. Our results also show that roadside $PM_{2.5}$ was up to 17% higher in holidays than in workdays in all the PRD cities except Hong Kong that showed roadside $PM_{2.5}$ higher in workdays than in holidays. The population-weighted $PM_{2.5}$ decreased with increasing distances from roads in every PRD city, and population-weighted $PM_{2.5}$ was estimated to be up to 22% higher at roadsides than at distances of 1500 m away from roads. This study pinpointed the seriousness of roadside air pollution in the PRD region.

1. Introduction

Particulate matter with an aerodynamic diameters $\leqslant$2.5 μm ($PM_{2.5}$) has been reported to be associated with health outcomes such as cardiovascular and respiratory diseases (Yim and Barrett 2012, Yim *et al* 2015, 2019b, 2022, Yang *et al* 2019, Gu *et al* 2020, Gong *et al* 2021). It is estimated that ambient air pollution caused 4.2 million premature deaths every year (Landrigan 2017). Air pollution has become a critical environmental problem especially in urban areas. This calls for urgent actions to address the problem for protecting population health.

Roadside $PM_{2.5}$ pollution and the resultant population exposure are major challenges in urban areas (Masiol *et al* 2017, Tong *et al* 2020, Wang *et al* 2020a). The difficulties to mitigate roadside $PM_{2.5}$ pollution are due to the substantial air pollutant emissions at roads and the complex surrounding physical environment. The emission sources along roadside comprise not only out-of-pipe exhaust emissions from vehicles but also non-exhaust particulate emissions from wear of tires, breaks, and road surfaces (Harrison *et al* 2021, Meng *et al* 2021, Zhou *et al* 2021, Fussell *et al* 2022). Moreover, building morphology in urban areas can reduce air ventilation along roadside, weakening air pollutant diffusion and trapping them within street canyons (Chan *et al* 2001, Kurppa *et al* 2018, Voordeckers *et al* 2021, Wang *et al* 2021). The complexity of roadside $PM_{2.5}$ pollution requires high-spatial-resolution-data to represent sufficient spatial scale for detailed analyses. Furthermore, assessing population $PM_{2.5}$ exposure requires to resolve $PM_{2.5}$ down to at least the road level in a city (Donkelaar *et al* 2015, Saraswat *et al* 2016, Wang *et al* 2019, 2022, Li *et al* 2021, Huang *et al* 2023). Roadside $PM_{2.5}$ measurements are typically sparse because of the limited space along roadside, low level of security for equipment installation and operation, and high cost of measurements, etc. The spatial distribution and population exposure of roadside $PM_{2.5}$ pollution on the city scale therefore cannot be fully evaluated.

Roadside $PM_{2.5}$ concentration can be measured by roadside stations and mobile sensors (Chen *et al* 2019, Suleiman *et al* 2019, Wadlow *et al* 2019, Xing *et al* 2019, Li *et al* 2020, Mukherjee *et al* 2020, Kakarla *et al* 2021, Afotey *et al* 2022), or simulated by atmospheric dispersion models (Tong *et al* 2020, Zhang *et al* 2022). Evaluating air pollution in a large urban agglomeration requires a certain level of spatial coverage. Remote sensing offers an alternative option such as Moderate Resolution Imaging Spectroradiometer (MODIS) (Lyapustin and Wang 2018), Advanced Himawari Imager (Yoshida *et al* 2018), Visible Infrared Imaging Radiometer Suite (Hsu *et al* 2019), and Landsat-8 Operational Land Imager (OLI) (Kaufman *et al* 1997a, Hsu *et al* 2006, 2013, 2017, Mhawish *et al* 2017, Yang *et al* 2018, 2022, Jin *et al* 2021, Tang *et al* 2021). To the best of our knowledge, remote sensing has not yet been adapted in roadside $PM_{2.5}$ analyses due to its coarse spatial resolution that was not fine enough for detailed roadside air pollution studies. One of the technological challenges for urban air pollution application is the Aerosol Optical Depth (AOD) retrieval for urban areas with a high radiance. This kind of challenge limited the further applications of satellite-retrieval approaches to roadside air pollution analyses.

This study aimed to assess the characteristics of roadside air pollution and the population-exposure in the Pearl River Delta (PRD) region (a large urban agglomeration with 11 cities) during 2014–2022 under clear sky conditions. We developed algorithms combined with the dark target (DT) method and machine learning to retrieve ground-level $PM_{2.5}$ in the PRD region based on Landsat-8 at a 30 m spatial resolution. We hence analysed the roadside $PM_{2.5}$ pollution in different cities and road types in the PRD region, evaluated the holiday and weekday characteristics and also estimated the population-exposure as a function of distance in different cities.

2. Materials and method

This study focused on analysing the roadside $PM_{2.5}$ in the PRD region, which is one of the most-developed urban agglomeration in China with a high population density, gross domestic product, and highway congestion index (Lang *et al* 2018, Hui *et al* 2020, Lin *et al* 2022). Despite significant efforts on air pollution control, the PRD region is still one of the major continental $PM_{2.5}$ source regions in China (Ji *et al* 2018, Lin *et al* 2018, Mai *et al* 2018). Haze problems remain a potential environmental hazard, especially under stable weather that can result in worse air quality and cause adverse public health impacts in the PRD region (Yim *et al* 2010, Filonchyk *et al* 2018, Luo *et al* 2018, Tong *et al* 2018a, 2018b, He *et al* 2019, Hou *et al* 2019, Yim *et al* 2019a, 2019b, Wang *et al* 2020b, 2020c, Huang *et al* 2021). Therefore, a detailed analysis of air pollution, especially roadside air pollution, should be conducted for the PRD region to provide a critical reference for formulating effective emission control policies.

To provide high-spatial-resolution $PM_{2.5}$ for our roadside $PM_{2.5}$ analyses, we developed 2-steps $PM_{2.5}$ retrieval algorithms based on Landsat-8. In the first step, we pre-processed the Landsat-8 level 1 data using radiation calibration, atmospheric correction, and cloud detection algorithms. Then we classified the pre-processed data into dense vegetation, water, and complex urban surface. To accurately extract the AOD from different areas, we applied the DT method (Kaufman *et al* 1997b) for vegetation and water surface. We then used these AOD results near the urban area as training data to estimate the AOD values over urban land surfaces with support vector machine (SVM) model (Cortes and Vapnik 1995). In the second step, we used random forest (RF) model (Breiman 2001) to analyse the AOD-$PM_{2.5}$ relationship along with auxiliary data including meteorological data, land-use data, and population data. These auxiliary data were carefully selected based on the relative importance test. The complete flowchart of the Landsat-8 $PM_{2.5}$ retrieval algorithms can be found in figure S1 in supplementary.

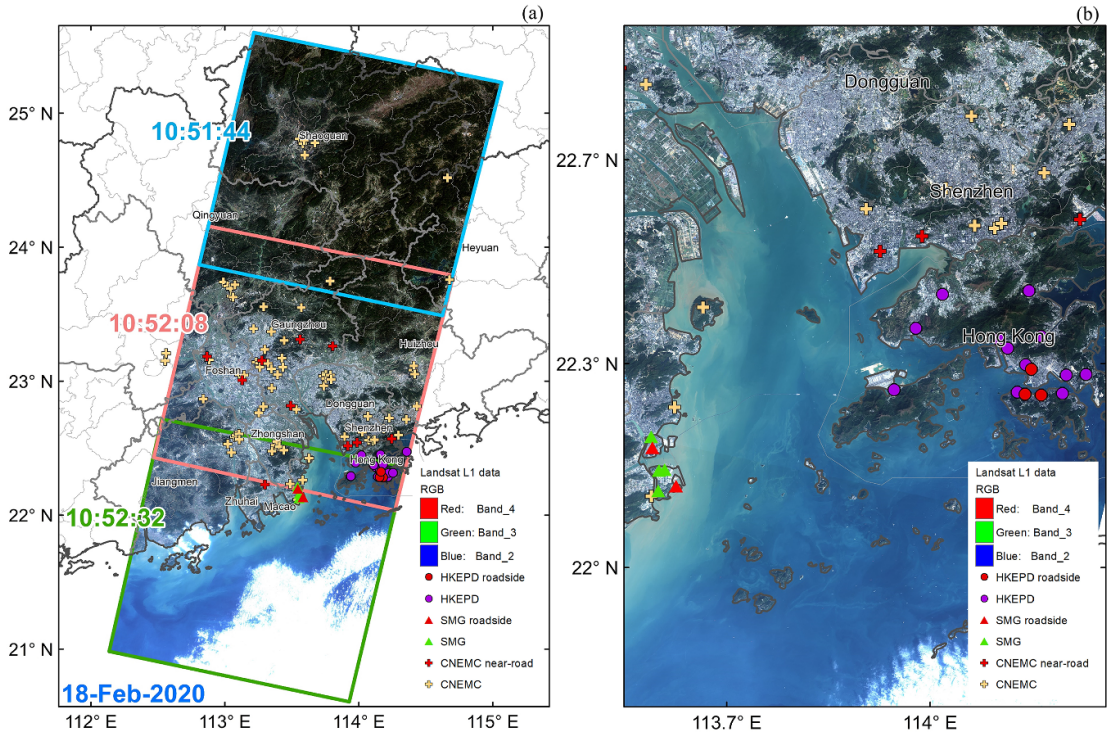

Figure 1. (a) Study area with Landsat-8 data and $PM_{2.5}$ ground stations (b) a zoomed map to show the dense $PM_{2.5}$ sites in Macao and Hong Kong. Reprinted from the National Geographic Information Resources Directory Service System. (www.webmap.cn).

2.1. Data

The Landsat-8 OLI/TIRS C1 Level-1 data were used for the AOD retrieval. Detailed parameters can be found in table S1. Three granules with a similar scene time inside the PRD region were chosen (figure 1). Any day during 2014–2022 with cloud coverage less than 30% in either of the first two Landsat-8 OLI granules (marked in blue and pink) were selected. As a result, 226 Landsat-8 data in the total of 77 d were selected.

Auxiliary data related to the AOD-$PM_{2.5}$ relationship model used in this study consisted of the 30 m Shuttle Radar Topography Mission 1 arc-second global elevation data, the 30 m Global land cover dataset (Globelland30) (Chen and Chen 2018), and the yearly 100 m WorldPop population distribution data (hub.worldpop.org). The meteorological data were obtained from ECMWF (https://cds.climate.copernicus.eu/) ERA5-Land hourly data with the continuous real-time gridded data measured at spatial resolutions of 0.1°, including 10 m U-component of wind ($m\,s^{-1}$), 10 m V-component of wind ($m\,s^{-1}$), 2 m temperature (K), surface net solar radiation ($J\,m^{-2}$), surface pressure (Pa), leaf area index with low vegetation ($m^2\,m^{-2}$), leaf area index with high vegetation ($m^2\,m^{-2}$), total evaporation (m.w.e meter of water equivalent) and total precipitation (m). The wind velocity ($m\,s^{-1}$) and direction (°) were also calculated using 10 m U and V components. The relative humidity (%) was calculated using the 2 m dewpoint temperature (K), 2 m temperature, and surface pressure data. To improve the accuracy and spatial resolution, we also combined the ECMWF grided data with hourly meteorological in-situ measurements from NOAA Integrated Surface Data lite data set (www.ncei.noaa.gov/pub/data/noaa/isd-lite/) including temperate, surface pressure, wind speed, and wind direction.

For AOD results validation, we used two sites with level 2.0 AOD AERONET data (Giles *et al* 2019) at 440 nm with a network of ground-based Sun photometers within ±1 h of the Landsat-8 scenes acquisition time. $PM_{2.5}$ results validation used $PM_{2.5}$ data at 62 stations obtained from China National Environmental Monitoring Centre (CNEMC) (http://106.37.208.233:20035/) measured by ambient air quality continuous automated monitoring system, at six stations from Macao Meteorological and Geophysical Bureau (SMG) (www.smg.gov.mo) measured with tapered element oscillating microbalance or beta ray attenuation method, and at 16 stations from Hong Kong Environmental Protection Department (HKEPD) (www.aqhi.gov.hk/) collected by continuous ambient air monitor.

It is noted that the $PM_{2.5}$ results validation included the roadside $PM_{2.5}$ measurements collected at two SMG roadside stations, nine near-road CNEMC stations (⩽10 m away from the edge of roads) and three HKEPD roadside stations.

The digital map obtained from Open Street Map (OSM) (www.openstreetmap.org) was utilized to

abstract the $PM_{2.5}$ concentration through 15 types of roads, including cycleway, footway, living road, motorway, path, pedestrian road, primary road, residential road, secondary road, service road, steps, tertiary, track road, trunk road, and unclassified road. The definitions and examples for each road type are provided in table S2.

2.2. AOD retrieval algorithm

The AOD retrieval algorithm was developed by combining the DT method with the SVM model. We first applied the DT method on vegetation and water surface, and then used the surrounding AOD results in the urban area as training data to estimate the AOD values over urban land surfaces. SVM model was chosen because of its ability to explain nonlinear relationships with small samples.

The detailed processes included pre-processing, classification, and modelling. Firstly, the raw Landsat 8 data were pre-processed using radiation calibration, atmospheric correction and cloud detection algorithms (Qiu *et al* 2019). Secondly, we removed the areas covered by clouds and the coastal areas, and classified the remaining data into dense vegetation, water, and complex urban surface. The surface reflectance of vegetation and water surfaces was dominated by groups of endmembers corresponding to water, soil, and vegetation. The DT method was thus applied to these two types of surfaces for the AOD estimation.

Regarding the AOD retrieving algorithm for urban surfaces, machine learning was chosen because the urban land cover is complex and always contains bright areas, which could highly affect the accuracy of the DT method. To avoid such uncertainty, we used the average AOD of vegetation and water surfaces near the urban area within 3×3 pixels as the training data to fit the relationship between AOD and Landsat-8 reflectance. Deep blue (0.440 μm), green (0.560 μm), near-infrared (0.865 μm), and shortwave infrared (2.200 μm) band were used as parameters. Pixels with more than three vegetation and water pixels nearby were chosen as samples to estimate the relationship within urban surface areas using the SVM model. To choose representative samples and improve algorithm efficiency over Landsat-8 urban areas with a complex morphology structure, we used simple linear iterative clustering (SLIC) super-pixels (Achanta *et al* 2012) to efficiently group similar pixels to include as many types of urban areas as possible. 1000 SLIC Super-pixels were first built (figure S4), whereas 10 sample pixels were chosen within each Super-pixel. The model was built and validated by 10-fold cross-validation (10-fold CV) to avoid the overfitting problem and then applied to all urban area pixels. More detailed information can be found in the Supporting Information (SI).

2.3. PM2.5-AOD relationship model

The RF model was applied to analyse the AOD-$PM_{2.5}$ relationship because it can predict both continuous and categorical features and determine the relative importance of each feature. All the Landsat-8 AOD results from 2014 to 2022 were used in this model. Overall, AOD results in 226 Landsat-8 images on 77 d in the study period were retrieved and used in our roadside $PM_{2.5}$ pollution analyses. For each day, two to three Landsat-8 granules were used, and the average AOD was calculated for the Landsat-8 scene-overlapping areas. Moreover, to further improve the model performance, auxiliary data related to the AOD-$PM_{2.5}$ relationship were also included in the model, such as land-use data, population data, and meteorological data. As shown in figure S5, all the parameters were analysed based on the relative importance of $PM_{2.5}$ and the collinear relationship between one another, according to the p-value of the F-test and the variance inflation factor method, respectively.

For $PM_{2.5}$ results validation, our retrieval $PM_{2.5}$ concentration was compared to ground-level measurements at 84 sites. Cubic spline interpolation was used with the coordinates of stations to match the interpolated values of our results. To avoid the common over-fitting problem, three kinds of cross-validation were conducted and cross-compared: (1) the 10-fold CV, in which 90% of the sample were randomly selected as training data, and the remaining 10% data were used for validation. This validation was repeated 10 times; (2) the cross-validation with a single station withheld (1-station left-out CV), in which one of the stations was taken turns to be withheld when building another model, and the modelled $PM_{2.5}$ results were then compared with the data of the withheld station; and (3) validation by the whole data set (whole validation), in which the model built based on all the $PM_{2.5}$ site data was applied to the Landsat-8 AOD retrievals to get the $PM_{2.5}$ ground level estimation.

3. Results and discussion

3.1. Results validation

Figure 2(a) shows the $PM_{2.5}$ of 10-18-2015 as an example, whereas the complete results during 2014–2022 are shown in figure S8. Before analysing roadside $PM_{2.5}$, we first intensively validated for our developed $PM_{2.5}$ retrieval algorithms in two parts: (1) AOD and (2) $PM_{2.5}$.

The retrieved AOD were validated using AERONET AOD. Figure S6 (a) shows the validation of AOD against AERONET AOD within ± 1 h of the Landsat-8 scenes acquisition time from two sites in Hong Kong. The overall R^2 and RMSE were 0.84 and 0.15 $\mu g\ m^{-3}$, respectively, indicating that our

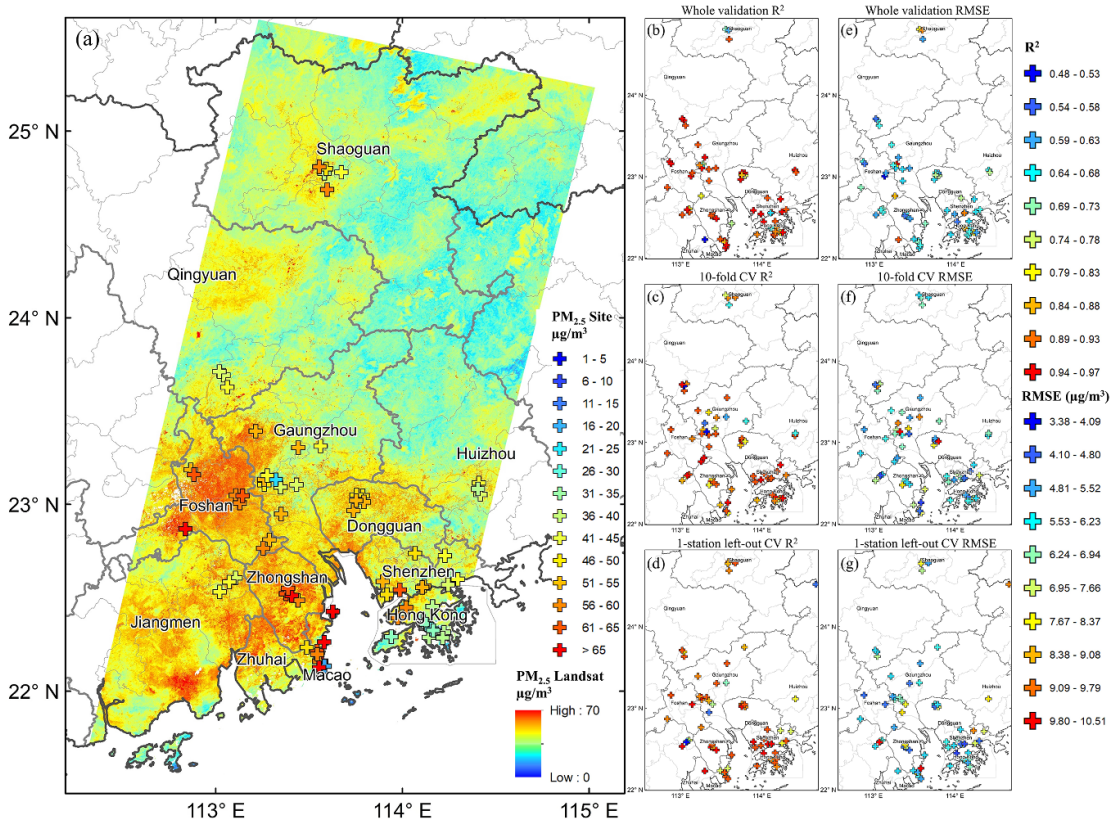

Figure 2. (a) A sample of spatial distribution of satellite-retrieval $PM_{2.5}$ concentration distribution ($\mu g\ m^{-3}$) on 10-18-2015; $PM_{2.5}$ R^2 among each station using model based on (b) whole validation (c) 10-fold CV and (d) 1-station left-out CV, and $PM_{2.5}$ RMSE ($\mu g\ m^{-3}$) among each station using model based on (e) whole validation (f) 10-fold CV and (g) 1-station left-out CV. Reprinted from the National Geographic Information Resources Directory Service System. (www.webmap.cn).

Landsat-8 AOD retrieval model was reliable. We also compared our AOD results with MODIS MAIAC AOD ($R^2 = 0.58$; RMSE = 0.14 $\mu g\ m^{-3}$), and the traditional DT method-retrieved AOD ($R^2 = 0.30$; RMSE = 0.19 $\mu g\ m^{-3}$), as shown in figure S6 (b). In addition, figure S7 compares the spatial patterns between MODIS MAIAC AOD and Landsat-8-derived AOD products on 15-10-2014 and 05-11-2016 as an example. The results indicate that both results had a similar spatial distribution; nevertheless, the Landsat-8 AOD contained more detailed spatial information.

We also compared our results with the hourly $PM_{2.5}$ ground-level measurements at 84 stations in the matching time (figures 2(b)–(g)). On average, R^2 and RMSE were estimated to be 0.86 and 7.72 $\mu g\ m^{-3}$, respectively. On the other hand, 10-fold CV shows $R^2 = 0.75$ and RMSE = 9.81 $\mu g\ m^{-3}$, whereas 1-station left-out CV shows $R^2 = 0.74$ and RMSE = 9.94 $\mu g\ m^{-3}$ (figure 3). In addition, we compared 1 km $PM_{2.5}$ product generated from MODIS MAIAC AOD products by (Wei *et al* 2019) (figures S9–S11). The results show R^2 and RMSE to be 0.72 and 10.0 $\mu g\ m^{-3}$, respectively. We also compared the range of our $PM_{2.5}$ estimation in each PRD city with all the $PM_{2.5}$ ground-level measurements. We selected the stationary data from 2014 to 2022 under clear sky condition with less than 30% cloud coverage and no precipitation. Figure S9 shows that the range of our $PM_{2.5}$ results in all 11 PRD cities was consistent with the $PM_{2.5}$ stationary data. The results above overall indicate that our results had a comparable accuracy and provided more spatial distribution details.

3.2. Roadside $PM_{2.5}$ analysis

With the 30 m $PM_{2.5}$ results, we analysed $PM_{2.5}$ distribution in the 11 cities in PRD region at the road level. Our retrieved $PM_{2.5}$ concentration was first overlaid onto OSM digital road data to extract roadside $PM_{2.5}$ on 15 types of roads. The definitions and examples for each road type can be found in table S2. Figure 4 depicts the highly polluted roads in each city as a demonstration. Our results show high $PM_{2.5}$ values often occurred in heavy traffic road types such as motorway, trunk, and primary roads. Within busy expressway roads, hot spots were often found in the middle part of roads due to high-speed car movement (e.g. up to 107.60 $\mu g\ m^{-3}$ on Motorway in Foshan, 103.99 $\mu g\ m^{-3}$ on Motorway in Zhuhai). On the contrary, within inner city roads, high $PM_{2.5}$ were often located at street intersections because of congestions, acceleration, and stop-and-go activities (e.g. up to 100.09 $\mu g\ m^{-3}$ on secondary road in Guangzhou, 90.71 $\mu g\ m^{-3}$ on living road in Shenzhen).

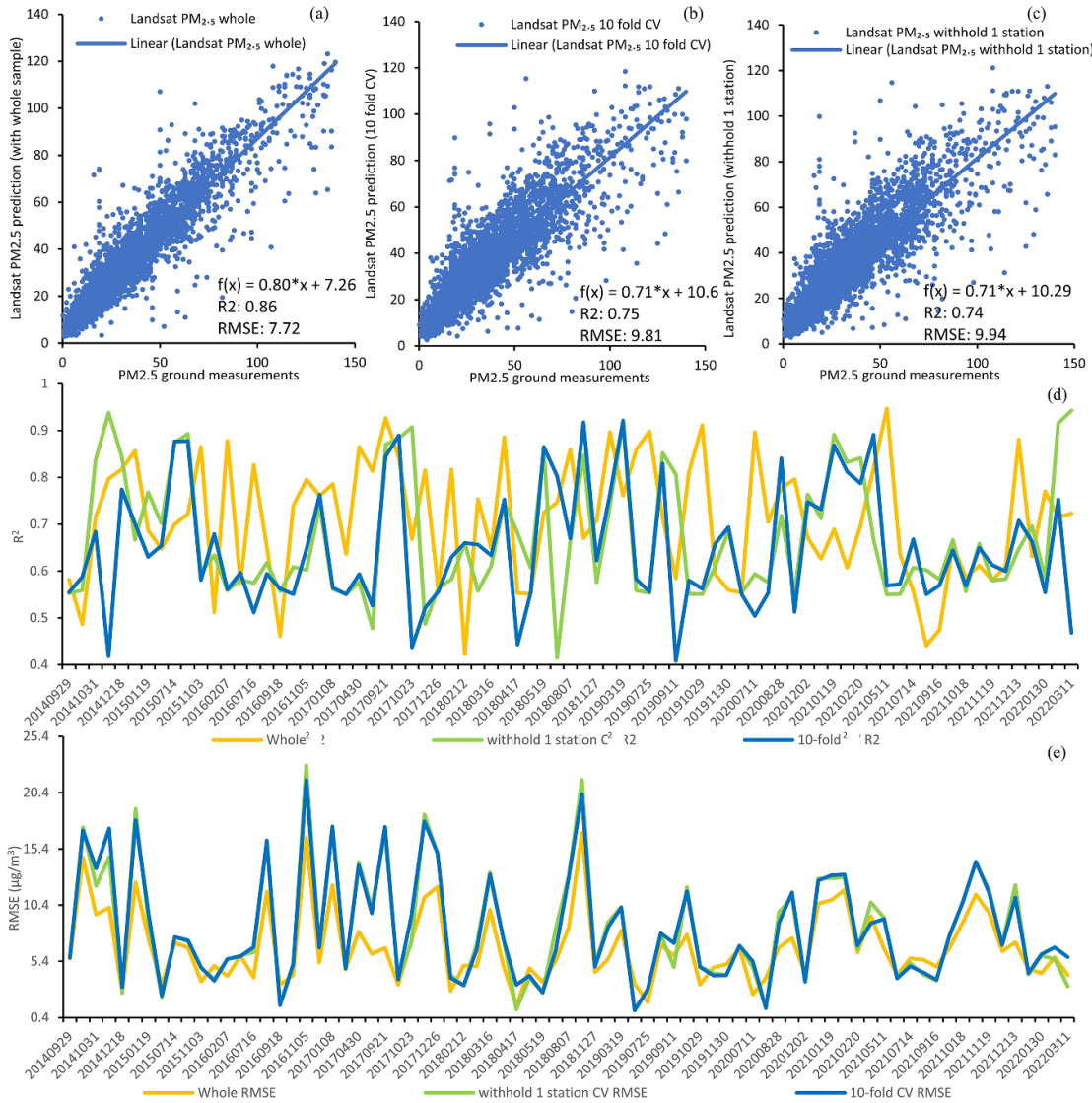

Figure 3. $PM_{2.5}$ validation results with all 84 $PM_{2.5}$ stations (R^2 and RMSE) for (a) whole validation, (b) 1-station left-out CV, (c) 10-fold CV; the R^2 (d) and RMSE (e) of the three types of validation in each day.

Considering the distribution difference within different parts of the roads, we applied the Monte Carlo method (Garcia *et al* 1987) to statistically evaluate the differences in roadside air pollution between different road types, cities, and dates. In each comparison, we randomly selected 1000 000 samples, and removed any insignificant results (p-value $\geqslant 0.05$). Comparing to averaging, our method can analyse the difference in $PM_{2.5}$ between roads on a more detailed level. The average $PM_{2.5}$ concentration for each road type, cities and dates can also be found in figure S15.

Figure 5(a) shows the difference in roadside $PM_{2.5}$ between each city. It notes that warmer colour in the vertical direction indicates higher $PM_{2.5}$ concentration whereas cooler colour means lower values. The average $PM_{2.5}$ concentration for each city and date were also provided in figure S16 in SI. Among all the cities in the PRD region, roads in traffic hub cities such as Foshan and Guangzhou were the most polluted, followed by surrounding cities such as Dongguan, Zhongshan, and Jiangmen. Meanwhile, Hong Kong's roads showed the lowest $PM_{2.5}$ concentration of 31.71 μg m^{-3} on average, almost 29.70% higher than the average value in Foshan. Seaside cities such as Shenzhen, Zhuhai and Macao were also relatively clean, with average $PM_{2.5}$ of 34.54 μg m^{-3}, 35.60 μg m^{-3}, and 36.48 μg m^{-3}, respectively. We also calculated the difference in $PM_{2.5}$ in each road type among each city. The difference in $PM_{2.5}$ between each city tended to be more obvious on roads for motorized vehicles, such as motorway, primary road, secondary road, and trunk road, and less noticeable on roads for non-motorized vehicles and pedestrians such as cycleway, footway, and track roads. This indicates that the $PM_{2.5}$ concentration level on non-motorized roads in most PRD cities were not dominated by traffic air pollution. Instead, they were likely to be dominated by background $PM_{2.5}$ level.

Figure 5(b) displays the differences in $PM_{2.5}$ among each road type in the PRD region. In general,

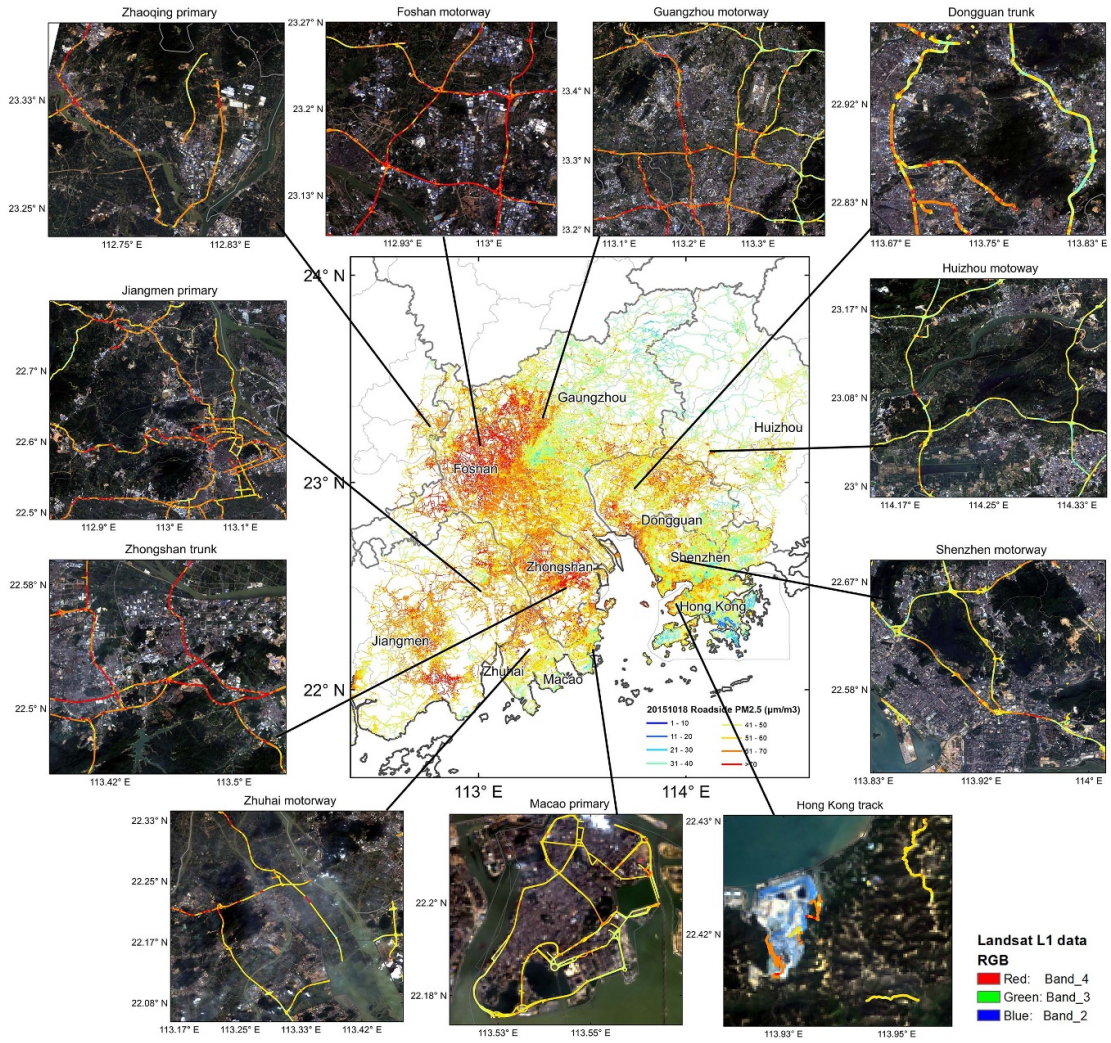

Figure 4. A sample of roadside $PM_{2.5}$ concentration ($\mu g\ m^{-3}$) over PRD in 10-18-2015 and of the road types in the 11 cities with the relatively high $PM_{2.5}$. Reprinted from the National Geographic Information Resources Directory Service System. (www.webmap.cn).

warmer colours on the vertical axis often appeared on road types related to motorized vehicles. Cooler colours with negative values often appeared on roads related to non-motorized vehicles and pedestrians, such as cycleway, footway, path, pedestrian, and steps. Average $PM_{2.5}$ higher than 37.00 $\mu g\ m^{-3}$ only occurred on motorized road types such as trunk, tertiary, motorway, primary, secondary, residential road, and living road. The highest $PM_{2.5}$ was observed on the trunk roads (38.98 $\mu g\ m^{-3}$ on average), whereas the lowest $PM_{2.5}$ was observed in road type of steps. The $PM_{2.5}$ level of trunk roads was 18% higher than that of the road type of steps, which were typically on hiking trails and more far away from main roads compared to cycleway and pedestrian roads.

We also analysed the differences in $PM_{2.5}$ among road types in each city (figure S17). In most cities in the region, the highest $PM_{2.5}$ appeared in primary roads, trunk, and motorways, which were usually major divided highways with 4–8 lanes. $PM_{2.5}$ on these roads were 9%–22% higher than that on the cleanest non-motorized roads. The highest $PM_{2.5}$ were located on motorway in Foshan (max: 107.60 $\mu g\ m^{-3}$; mean: 48.03 $\mu g\ m^{-3}$). In Hong Kong, tracks roads had the highest $PM_{2.5}$ (max: 85.10 $\mu g\ m^{-3}$; mean: 33.54 $\mu g\ m^{-3}$), which were 12% higher than the average $PM_{2.5}$ on step roads. Track roads were usually routes that were separated from traffic, but several hot spots (figure S18) were found in track roads contributing to high air pollution, such as the one inside the WENT (West New Territories) landfill, and the road outside of an asphalt company, which has already been convicted and fined by the government for violating the Air Pollution Control Ordinance license conditions.

Figure 5(c) depicts the differences in $PM_{2.5}$ between holidays and workdays in each road type and city according to different local laws in mainland China, Hong Kong, and Macao. According to the figure, Hong Kong was the only city with higher $PM_{2.5}$

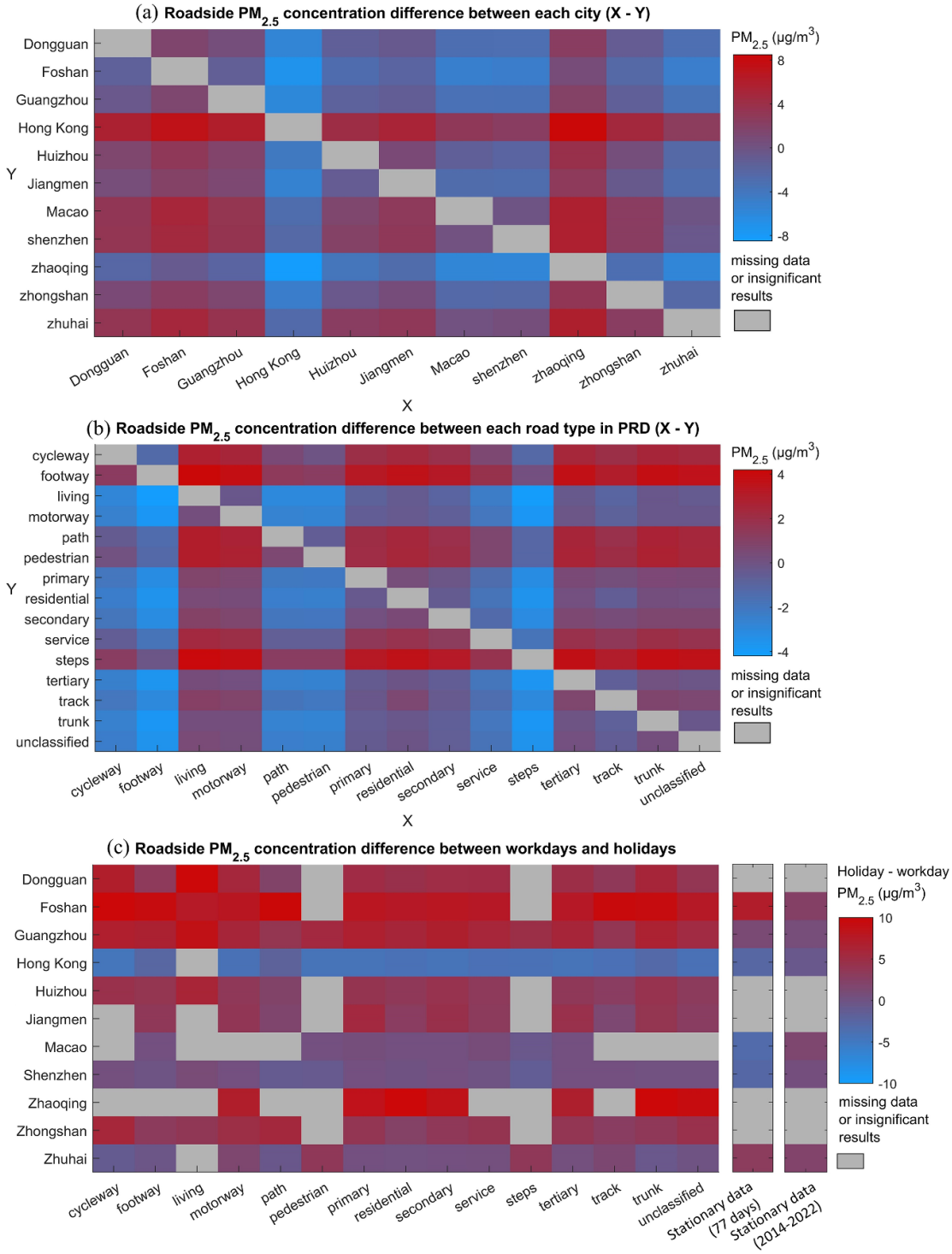

Figure 5. Roadside $PM_{2.5}$ comparison ($\mu g\ m^{-3}$) between (a) the PRD 11 cities; (b) 15 road types in the PRD region; (c) workdays and holidays in each road type and in each PRD city. In (c), the last two columns show the results based on the data collected at ground level stations.

concentration (1.93–4.50 $\mu g\ m^{-3}$) during workdays, whereas $PM_{2.5}$ level remained the same between holidays and workdays in Shenzhen, Zhuhai, and Macao. In the rest of PRD cities, $PM_{2.5}$ concentration in holidays were 8%–17% higher than that in workdays. To prove our findings, we also calculated the holiday-workday differences in $PM_{2.5}$ using the roadside $PM_{2.5}$ measurements with the same time periods of our retrieval $PM_{2.5}$ data. The roadside data measurements show comparable results with the satellite retrieved data showing larger differences in $PM_{2.5}$ between holiday and workday. The holiday-workday pattern could be because tourists in Hong Kong may prefer to use the advanced public transfer system inside the city, whereas people in mainland China tended to drive between cities on holidays; the other

reason could be Hong Kong cross-border trucking with mainland China on workdays was busier than on holidays. To further understand the traffic pattern, we evaluated the traffic volume data in Hong Kong and Shenzhen (figure S21). It shows that the traffic volume in Hong Kong was almost 30% higher on holidays then on workdays, whereas Shenzhen shows negligible difference in its traffic volume between holidays and workdays. This is consistent with our results. It is noted that our analysis focused on clear-sky condition, whereas traffic volume may reduce during severe weather conditions (Miao *et al* 2019, Akter *et al* 2020).

Moreover, we calculate the roadside the population-weighted $PM_{2.5}$ exposure using the formula $\sum(P_i * C_i)/\sum P_i$, where P_i is the population and C_i is the $PM_{2.5}$ concentration. We analysed the population-weighted $PM_{2.5}$ as a function of distance from roads starting from 0 m to 1500 m in the PRD region and in each city. This analysis only considered the roads for motorized vehicles with high $PM_{2.5}$ including motorway, primary, residential, secondary, service, tertiary, track, trunk and unclassified roads. We calculated the distance between each pixel within boundary of each city and the nearest road (figure S19), and then calculated the average population-weighted $PM_{2.5}$ within each 30 m distance ring from roads.

Figure 6 shows that the population-weighted $PM_{2.5}$ tended to decrease with the increasing distance from roads in the whole PRD region and in each city. Among all the PRD cities, Dongguan, Foshan, Zhongshan and Jiangmen had relatively high population-weighted $PM_{2.5}$ near roads. Guangzhou had a comparable level of population-weighted $PM_{2.5}$ within 200 m from roads, and then the population-weighted $PM_{2.5}$ declined sharply and became the second last after 1 km from roads. Similar to Guangzhou, Shenzhen and Hong Kong show the similar sharp reduction in population-weighted $PM_{2.5}$ after several meters from roads. This characteristic clearly reflected the critical impacts of the traffic emissions to the air pollution near roads in the cities. On the other hand, Zhuhai had relative marginal changes along distances from roads due to its relatively less traffic. The stable level of population-weighted $PM_{2.5}$ reflected the minor contribution of traffic emissions to the air quality in Zhuhai.

Our results also show that the population-weighted $PM_{2.5}$ profiles of the PRD region and most of the PRD cities (8 out of 11) had an increase within 100 m from roads. The slight increases in population-weighted $PM_{2.5}$ indicate that the traffic pollution tended to accumulate within a certain distance, and there might be a heightened population-weighted $PM_{2.5}$ zone near the roads. Overall, the population-weighted $PM_{2.5}$ was 2%–22% higher at roadsides than at distances more than 1500 m away from roads in the PRD region.

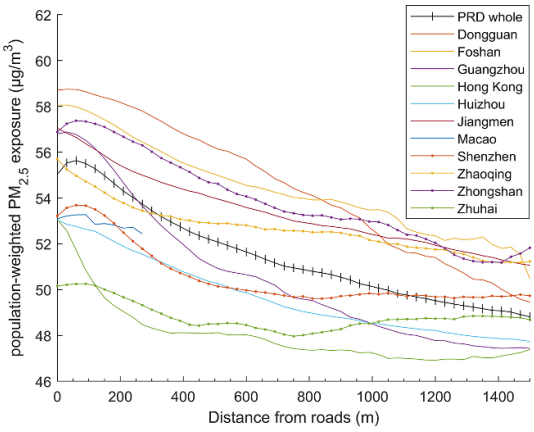

Figure 6. The averaged population-weighted $PM_{2.5}$ ($\mu g\ m^{-3}$) as a function of distance from roads starting from 0 m to 1500 m in the PRD region and in each city. The values in each distance point were averaged in a 30 m distance interval.

3.3. Future research

This study provided a comprehensive analysis of roadside $PM_{2.5}$ distribution and the resultant population exposure. It should be noted that evaluating the contribution of traffic-related emissions to roadside $PM_{2.5}$ is critical. Future studies are recommended to conduct a source apportionment study to assess the contribution of vehicular emissions and the background $PM_{2.5}$ to the roadside $PM_{2.5}$ in various cities. Additionally, we plan to enhance the temporal resolution of our results by combining multiple satellite sources. These proposed improvements are anticipated to further enhance our understanding of roadside $PM_{2.5}$ distribution.

4. Conclusions

This study developed Landsat-8 $PM_{2.5}$ retrieval algorithms to derive $PM_{2.5}$ concentration at 30 m spatial resolution over the PRD region and applied the retrieval $PM_{2.5}$ results to analyse roadside air pollution in the PRD cities. The Landsat-8 retrieval AOD results show a better relationship with AERONET AODs compared to the traditional DT method and MODIS 1 km MAIAC AOD products. In addition, our $PM_{2.5}$ estimation shows a good relationship with $PM_{2.5}$ ground-level measurements including those at roadside stations. Our roadside pollution analyses show that the roadside $PM_{2.5}$ in Dongguan, Foshan, Guangzhou, Zhaoqing and Zhongshan were relatively higher, whereas that in Hong Kong was relatively lower. The high roadside $PM_{2.5}$ typically occurred at roads for motorized vehicles, such as, motorway, trunk, primary roads, secondary roads, and tertiary roads. Furthermore, roadside $PM_{2.5}$ was also higher in holidays than workdays in the PRD region except for Hong Kong which shows an opposite result. This was consistent with traffic volume data. Additionally, we found that the population-weighted

$PM_{2.5}$ decreased with the increasing distances from roads in the whole PRD area, and serious roadside $PM_{2.5}$ pollution was clearly shown in some cities. The decline rate appeared to reduce and to even stabilize in the areas more than 1 km away from roads, suggesting that areas far away from roads may be less influenced by traffic emissions. This study underscored the adverse roadside $PM_{2.5}$ pollution in the PRD region.

Data availability statement

The data cannot be made publicly available upon publication because they are not available in a format that is sufficiently accessible or reusable by other researchers. The data that support the findings of this study are available upon reasonable request from the authors.

Acknowledgments

The authors would like to thank for the following grants for their supports on this research: Start-up Grant from NTU (SUG: 021384-00001) and Ministry of Education of Singapore (MOE SUG: 021452-00001), MOE AcRF Tier 1 from Ministry of Education of Singapore (RG126/21: 021591-00001), EOS FY2022 funding (EOS MOE RCE FY 2022: 021943-0001) from Earth Observatory of Singapore at NTU and Dr Stanley Ho Medical Development Foundation (Grant No. 8305509).

ORCID iDs

Y Wu https://orcid.org/0000-0002-1678-6509
H F Lee https://orcid.org/0000-0001-5415-7845
S H L Yim https://orcid.org/0000-0002-2826-0950

References

Achanta R, Shaji A, Smith K, Lucchi A, Fua P and Süsstrunk S 2012 SLIC superpixels compared to state-of-the-art superpixel methods *IEEE Trans. Pattern Anal. Mach. Intell.* **34** 2274–81

Afotey B, Sattler M, Parsaeifard N, Pearson Y E, Chakraborty M and Hada S 2022 Impact of corona virus stay-at-home policies on traffic emissions and ambient pollutant concentrations in Ghana, West Africa *Eng. Sci.* **17** 285–91

Akter T, Mitra S K, Hernandez S and Corro-Diaz K 2020 A spatial panel regression model to measure the effect of weather events on freight truck traffic *Transportmetrica* A **16** 910–29

Breiman L 2001 Random forests *Mach. Learn.* **45** 5–32

Chan A T, So E S P and Samad S C 2001 Strategic guidelines for future development to achieve sustainable air quality in urban area *Atmos. Environ.* **35** 5681–91

Chen J and Chen J 2018 GlobeLand30: operational global land cover mapping and big-data analysis *Sci. China Earth Sci.* **61** 1533–4

Chen S, Zhang X, Lin J, Huang J, Zhao D, Yuan T and Xie L 2019 Fugitive road dust $PM_{2.5}$ emissions and their potential health impacts *Environ. Sci. Technol.* **53** 8455–65

Cortes C and Vapnik V 1995 *Support-vector Networks Machine Learning* vol 20 (Kluwer Academic Publisher) pp 237–97

Donkelaar A V, Martin R V, Brauer M and Boys B L 2015 Use of satellite observations for long-term exposure assessment of global concentrations of fine particulate matter *Environ. Health Perspect.* **123** 135–43

Filonchyk M, Yan H and Zhang Z 2018 Analysis of spatial and temporal variability of aerosol optical depth over China using MODIS combined dark target and deep blue product *Theor. Appl. Climatol.* **137** 2271–88

Fussell J C, Franklin M, Green D C, Gustafsson M, Harrison R M, Hicks W and Zhu Y 2022 A review of road traffic-derived non-exhaust particles: emissions, physicochemical characteristics, health risks, and mitigation measures *Environ. Sci. Technol.* **56** 6813–35

Garcia A L, van den Broeck C, Aertsens M and Serneels R 1987 A Monte Carlo simulation of coagulation *Physica* A **143** 535–46

Giles D M, Sinyuk A, Sorokin M G, Schafer J S, Smirnov A, Slutsker I and Lyapustin A I 2019 Advancements in the Aerosol Robotic Network (AERONET) Version 3 database—automated near-real-time quality control algorithm with improved cloud screening for Sun photometer aerosol optical depth (AOD) measurements *Atmos. Meas. Technol.* **12** 169–209

Gong K, Li L, Li J, Qin M, Wang X, Ying Q and Hu J 2021 Quantifying the impacts of inter-city transport on air quality in the Yangtze River Delta urban agglomeration, China: implications for regional cooperative controls of $PM_{2.5}$ and O_3 *Sci. Total Environ.* **779** 146619

Gu Y, Zhang W, Yang Y, Wang C, Streets D G and Yim S H L 2020 Assessing outdoor air quality and public health impact attributable to residential black carbon emissions in rural China *Resour. Conserv. Recycl.* **159** 104812

Harrison R M, Vu T V, Jafar H and Shi Z 2021 More mileage in reducing urban air pollution from road traffic *Environ. Int.* **149** 106329

He Q, Gu Y and Zhang M 2019 Spatiotemporal patterns of aerosol optical depth throughout China from 2003 to 2016 *Sci. Total Environ.* **653** 23–35

Hou X, Chan C K, Dong G H and Yim S H L 2019 Impacts of transboundary air pollution and local emissions on $PM_{2.5}$ pollution in the Pearl River Delta region of China and the public health, and the policy implications *Environ. Res. Lett.* **14** 034005

Hsu N C, Jeong M J, Bettenhausen C, Sayer A M, Hansell R, Seftor C S and Tsay S C 2013 Enhanced Deep Blue aerosol retrieval algorithm: the second generation *J. Geophys. Res. Atmos.* **118** 9296–315

Hsu N C, Lee J, Sayer A M, Carletta N, Chen S H, Tucker C J and Tsay S C 2017 Retrieving near-global aerosol loading over land and ocean from AVHRR *J. Geophys. Res. Atmos.* **122** 9968–89

Hsu N C, Lee J, Sayer A M, Kim W, Bettenhausen C and Tsay S-C 2019 VIIRS Deep Blue aerosol products over land: extending the EOS long-term aerosol data records *J. Geophys. Res. Atmos.* **124** 4026–53

Hsu N C, Tsay S-C, King M D and Herman J R 2006 Deep blue retrievals of Asian aerosol properties during ACE-Asia *IEEE Trans. Geosci. Remote Sens.* **44** 3180–95

Huang G, Huang X, Liu C, Wu L, Liu G, Xing Y and Yan M 2023 Characterizing spatiotemporal patterns of elevated PM2.5 exposures in a megacity of China using combined mobile and stationary measurements *Atmos. Environ.* **307** 119821

Huang T, Yang Y, O'Connor E J, Lolli S, Haywood J, Osborne M and Yim S H L 2021 Influence of a weak typhoon on the vertical distribution of air pollution in Hong Kong: a perspective from a Doppler LiDAR network *Environ. Pollut.* **276** 116534

Hui E C M, Li X, Chen T and Lang W 2020 Deciphering the spatial structure of China's megacity region: a new bay area—The Guangdong-Hong Kong-Macao Greater Bay Area in the making *Cities* **105** 102168

Ji G, Zhao J, Yang X, Yue Y and Wang Z 2018 Exploring China's 21-year PM 10 emissions spatiotemporal variations by

DMSP-OLS nighttime stable light data] *Atmos. Environ.* **191** 132–41

Jin Y, Hao Z, Chen J, He D, Tian Q, Mao Z and Pan D 2021 Retrieval of urban aerosol optical depth from landsat 8 OLI in Nanjing, China *Remote Sens.* **13** 415

Kakarla A, Munagala V S K R, Ishizaka T, Fukuda A and Jana S 2021 Spatiooral prediction of roadside $PM_{2.5}$ based on sparse mobile sensing and traffic information *27th National Conf. on Communications, NCC 2021*

Kaufman Y J, Tanre D, Remer L A, Vermote E F, Chu A and Holben B N 1997a Operational remote sensing of tropospheric aerosol over land from EOS moderate resolution imaging spectroradiometer *J. Geophys. Res.* **102** 17051–67

Kaufman Y J, Wald A E, Remer L A, Bo-Cai G, Rong-Rong L and Flynn L 1997b The MODIS 2.1-mum channel-correlation with visible reflectance for use in remote sensing of aerosol *IEEE Trans. Geosci. Remote Sens.* **35** 1286–98

Kurppa M, Hellsten A, Auvinen M, Raasch S, Vesala T and Järvi L 2018 Ventilation and air quality in city blocks using large-eddy simulation—urban planning perspective *Atmosphere* **9** 65

Landrigan P J 2017 Air pollution and health *Lancet Public Health* **2** e4–e5

Lang W, Long Y and Chen T 2018 Rediscovering Chinese cities through the lens of land-use patterns *Land Use Policy* **79** 362–74

Li X, Yang T, Zeng Z, Li X, Zeng G, Liang J and Chen X 2021 Underestimated or overestimated? Dynamic assessment of hourly $PM_{2.5}$ exposure in the metropolitan area based on heatmap and micro-air monitoring stations *Sci. Total Environ.* **779** 146283

Li Z, Yim S H L and Ho K F 2020 High temporal resolution prediction of street-level $PM_{2.5}$ and NOx concentrations using machine learning approach *J. Clean. Prod.* **268** 121975

Lin C, Li Y, Lau A K H, Li C and Fung J C H 2018 15-year $PM_{2.5}$ trends in the pearl river delta region and Hong Kong from satellite observation *Aerosol Air Qual. Res.* **18** 2355–62

Lin P, He Y, Pei M and Yang R 2022 Data-driven spatial-temporal analysis of highway traffic volume considering weather and festival impacts *Travel Behav. Soc.* **29** 95–112

Luo M, Hou X, Gu Y, Lau N C and Yim S H L 2018 Trans-boundary air pollution in a city under various atmospheric conditions *Sci. Total Environ.* **618** 132–41

Lyapustin A and Wang Y 2018 MCD19A2 MODIS/Terra+ aqua land aerosol optical depth daily L2G global 1km SIN grid V006 *NASA EOSDIS land processes DAAC* (https://doi.org/10.5067/MODIS/MCD19A2.006)

Mai B, Deng X, Li Z, Liu J, Xia X, Che H and Cribb M 2018 Aerosol optical properties and radiative impacts in the Pearl River Delta region of China during the dry season *Adv. Atmos. Sci.* **35** 195–208

Masiol M, Hopke P K, Felton H D, Frank B P, Rattigan O V, Wurth M J and LaDuke G H 2017 Source apportionment of PM2.5 chemically speciated mass and particle number concentrations in New York City *Atmos. Environ.* **148** 215–29

Meng M R, Cao S J, Kumar P, Tang X and Feng Z 2021 Spatial distribution characteristics of PM2.5 concentration around residential buildings in urban traffic-intensive areas: from the perspectives of health and safety *Saf. Sci.* **141** 105318

Mhawish A, Banerjee T, Broday D M, Misra A and Tripathi S N 2017 Evaluation of MODIS Collection 6 aerosol retrieval algorithms over Indo-Gangetic Plain: implications of aerosols types and mass loading *Remote Sens. Environ.* **201** 297–313

Miao Q, Welch E W and Sriraj P S 2019 Extreme weather, public transport ridership and moderating effect of bus stop shelters *J. Transp. Geogr.* **74** 125–33

Mukherjee A, McCarthy M C, Brown S G, Huang S, Landsberg K and Eisinger D S 2020 Influence of roadway emissions on near-road PM2.5: monitoring data analysis and implications *Transp. Res.* D **86** 102442

Qiu S, Zhu Z and He B 2019 Fmask 4.0: improved cloud and cloud shadow detection in Landsats 4–8 and Sentinel-2 imagery *Remote Sens. Environ.* **231** 111205

Saraswat A, Kandlikar M, Brauer M and Srivastava A 2016 $PM_{2.5}$ population exposure in New Delhi using a probabilistic simulation framework *Environ. Sci. Technol.* **50** 3174–83

Suleiman A, Tight M R and Quinn A D 2019 Applying machine learning methods in managing urban concentrations of traffic-related particulate matter (PM_{10} and $PM_{2.5}$) *Atmos. Pollut. Res.* **10** 134–44

Tang Y, Deng R, Li J, Liang Y, Xiong L, Liu Y and Hua Z 2021 Estimation of ultrahigh resolution pm2.5 mass concentrations based on mie scattering theory by using landsat8 oli images over pearl river delta *Remote Sens.* **13** 2463

Tong C H M, Yim S H L, Rothenberg D, Wang C, Lin C Y, Chen Y D and Lau N C 2018a Assessing the impacts of seasonal and vertical atmospheric conditions on air quality over the Pearl River Delta region *Atmos. Environ.* **180** 69–78

Tong C H M, Yim S H L, Rothenberg D, Wang C, Lin C Y, Chen Y D and Lau N C 2018b Projecting the impacts of atmospheric conditions under climate change on air quality over the Pearl River Delta region *Atmos. Environ.* **193** 79–87

Tong R, Liu J, Wang W and Fang Y 2020 Health effects of $PM_{2.5}$ emissions from on-road vehicles during weekdays and weekends in Beijing, China *Atmos. Environ.* **223** 117258

Voordeckers D, Meysman F J R, Billen P, Tytgat T and Van Acker M 2021 The impact of street canyon morphology and traffic volume on NO_2 values in the street canyons of Antwerp *Build. Environ.* **197** 107825

Wadlow I, Paton-Walsh C, Forehead H, Perez P, Amirghasemi M, Guérette É A and Kumar P 2019 Understanding spatial variability of air quality in Sydney: part 2-a roadside case study *Atmosphere* **10** 217

Wang B, Li Y, Tang Z, Cai N and Niu H 2021 Effects of vehicle emissions on the $PM_{2.5}$ dispersion and intake fraction in urban street canyons *J. Clean. Prod.* **324** 129212

Wang B, Wu J, Xu X and Li Y 2022 Hourly population exposure index for $PM_{2.5}$ in urban street canyons *Urban Clim.* **45** 101242

Wang H, He X, Liang X, Choma E F, Liu Y, Shan L and Evans J S 2020a Health benefits of on-road transportation pollution control programs in China *Proc. Natl Acad. Sci.* **117** 25370–7

Wang H, Li J, Gao Z, Yim S H L, Shen H, Ho H C and Yang Y 2019 High-spatial-resolution population exposure to $PM_{2.5}$ pollution based on multi-satellite retrievals: a case study of seasonal variation in the Yangtze River Delta, China in 2013 *Remote Sens.* **11** 2724

Wang M Y, Yim S H L, Dong G H, Ho K F and Wong D C 2020b Mapping ozone source-receptor relationship and apportioning the health impact in the Pearl River Delta region using adjoint sensitivity analysis *Atmos. Environ.* **222** 117026

Wang Y, Yim S H L, Yang Y and Morin C W 2020c The effect of urbanization and climate change on the mosquito population in the Pearl River Delta region of China *Int. J. Biometeorol.* **64** 501–12

Wei J, Huang W, Li Z, Xue W, Peng Y, Sun L and Cribb M 2019 Estimating 1-km-resolution PM2.5 concentrations across China using the space-time random forest approach *Remote Sens. Environ.* **231** 111221

Xing Y, Brimblecombe P and Ning Z 2019 Fine-scale spatial structure of air pollutant concentrations along bus routes *Sci. Total Environ.* **658** 1–7

Yang B Y, Guo Y, Morawska L, Bloom M S, Markevych I, Heinrich J and Dong G H 2019 Ambient PM 1 air pollution and cardiovascular disease prevalence: insights from the 33 Communities Chinese health study *Environ. Int.* **123** 310–7

Yang F, Wang Y, Tao J, Wang Z, Fan M, de Leeuw G and Chen L 2018 Preliminary investigation of a new AHI aerosol optical depth (AOD) retrieval algorithm and evaluation with

multiple source AOD measurements in China *Remote Sens.* **10** 748

Yang Q, Yuan Q and Li T 2022 Ultrahigh-resolution $PM_{2.5}$ estimation from top-of-atmosphere reflectance with machine learning: theories, methods, and applications *Environ. Pollut.* **306** 119347

Yim S H L and Barrett S R H 2012 Public health impacts of combustion emissions in the United Kingdom *Environ. Sci. Technol.* **46** 4291–6

Yim S H L, Fung J C H and Lau A K H 2010 Use of high-resolution MM5/CALMET/CALPUFF system: SO2 apportionment to air quality in Hong Kong *Atmos. Environ.* **44** 4850–8

Yim S H L, Hou X, Guo J and Yang Y 2019a Contribution of local emissions and transboundary air pollution to air quality in Hong Kong during El Niño-Southern oscillation and heatwaves *Atmos. Res.* **218** 50–58

Yim S H L, Huang T, Ho J M W, Lam A S M, Yau S T Y, Yuen T W H and Sung J J Y 2022 Rise and fall of lung cancers in relation to tobacco smoking and air pollution: a global trend analysis from 1990 to 2012 *Atmos. Environ.* **269** 118835

Yim S H L, Wang M, Gu Y, Yang Y, Dong G and Li Q 2019b Effect of urbanization on ozone and resultant health effects in the Pearl River Delta Region of China *J. Geophys. Res. Atmos.* **124** 11568–79

Yim S H, Lee G L, Lee I H, Allroggen F, Ashok A, Caiazzo F, Eastham S D, Malina R and Barrett S R 2015 Global, regional and local health impacts of civil aviation emissions *Environ. Res. Lett.* **10** 034001

Yoshida M, Kikuchi M, Nagao T M, Murakami H, Nomaki T and Higurashi A 2018 Common retrieval of aerosol properties for imaging satellite sensors *J. Meteorol. Soc. Jpn.* II **96B** 193–209

Zhang B, Cheng S, Lu F and Lei M 2022 Estimation of exposure and premature mortality from near-roadway fine particulate matter concentrations emitted by heavy-duty diesel trucks in Beijing *Environ. Pollut.* **311** 119990

Zhou L, Salvador C M, Priestley M, Hallquist M, Liu Q, Chan C K and Hallquist Å M 2021 Emissions and secondary formation of air pollutants from modern heavy-duty trucks in real-world traffic—chemical characteristics using on-line mass spectrometry *Environ. Sci. Technol.* **55** 14515–25